NeuroImage 90 (2014) 423–435

Contents lists available at ScienceDirect

NeuroImage

journal homepage: www.elsevier.com/locate/ynimg

Exploring mechanisms of spontaneous functional connectivity in MEG: How delayed network interactions lead to structured amplitude envelopes of band-pass filtered oscillations ☆

Joana Cabral [a,b,*], Henry Luckhoo [c,d], Mark Woolrich [c], Morten Joensson [b,e], Hamid Mohseni [b], Adam Baker [c,d], Morten L. Kringelbach [b,e], Gustavo Deco [a,f]

[a] Theoretical and Computational Neuroscience Group, Center of Brain and Cognition, Universitat Pompeu Fabra, 08018 Barcelona, Spain
[b] Department of Psychiatry, University of Oxford, OX3 7JX Oxford, UK
[c] Oxford Centre for Human Brain Activity, University of Oxford, OX3 7JX Oxford, UK
[d] Centre for Doctoral Training in Healthcare Innovation, Institute of Biomedical Engineering, Department of Engineering Science, University of Oxford, OX1 3PJ Oxford, UK
[e] CFIN/MindLab, Aarhus University, 8000 Aarhus, Denmark
[f] Institució Catalana de Recerca i Estudis Avançats (ICREA), 08010 Barcelona, Spain

ARTICLE INFO

Article history:
Accepted 27 November 2013
Available online 7 December 2013

Keywords:
Resting state
MEG
Oscillations
Network
Kuramoto
Modeling
Structural connectivity
Functional connectivity

ABSTRACT

Spontaneous (or *resting-state*) brain activity has attracted a growing body of neuroimaging research over the last decades. Whole-brain network models have proved helpful to investigate the source of slow (<0.1 Hz) correlated hemodynamic fluctuations revealed in fMRI during rest. However, the mechanisms mediating resting-state long-distance correlations and the relationship with the faster neural activity remain unclear. Novel insights coming from MEG studies have shown that the amplitude envelopes of alpha- and beta-frequency oscillations (~8–30 Hz) display similar correlation patterns as the fMRI signals.

In this work, we combine experimental and theoretical work to investigate the mechanisms of spontaneous MEG functional connectivity. Using a simple model of coupled oscillators adapted to incorporate realistic whole-brain connectivity and conduction delays, we explore how slow and structured amplitude envelopes of band-pass filtered signals – fairly reproducing MEG data collected from 10 healthy subjects at rest – are generated spontaneously in the space-time structure of the brain network.

Our simulation results show that the large-scale neuroanatomical connectivity provides an optimal network structure to support a regime with metastable synchronization. In this regime, different subsystems may temporarily synchronize at reduced collective frequencies (falling in the 8–30 Hz range due to the delays) while the global system never fully synchronizes. This mechanism modulates the frequency of the oscillators on a slow time-scale (<0.1 Hz) leading to structured amplitude fluctuations of band-pass filtered signals. Taken overall, our results reveal that the structured amplitude envelope fluctuations observed in resting-state MEG data may originate from spontaneous synchronization mechanisms naturally occurring in the space-time structure of the brain.

Introduction

The biophysical mechanisms mediating spontaneous long-distance functional connectivity remain unclear. Typically, resting-state functional connectivity is evaluated using functional MRI from resting subjects (rs-fMRI) (Biswal et al., 1995, 2010) and quantified by determining the brain areas that exhibit correlated BOLD (Blood Oxygen-Level Dependent) signal fluctuations. A number of studies in theoretical and computational neuroscience have developed whole-brain models of spontaneous activity to investigate the origin of rs-fMRI functional connectivity and its relationship with the underlying white-matter structural connectivity. In general, models consist in a whole-brain network, where the nodes represent brain areas in the spontaneous state and the links represent the (excitatory) connections between them. Links are typically scaled in proportion to the number of white-matter fibers detected between areas, using the so-called structural connectome (Hagmann et al., 2007). At the node level, the spontaneous dynamics is represented using either neural mass models (Honey et al., 2007, 2009), mean field models (Cabral et al., 2011; Deco et al., 2009, 2013; Ghosh et al., 2008a, 2008b) or even realistic spiking/synaptic models (Deco and Jirsa, 2012). An important common feature of resting-state models is that the emergence of structured BOLD signal fluctuations is obtained when the model parameters are such that the system operates at the edge of a bifurcation. At this critical working

* Corresponding author at: Roc Boronat, 138, 08018 Barcelona, Spain.
E-mail address: joana.cabral@upf.edu (J. Cabral).

1053-8119/$ – see front matter © 2013 The Authors. Published by Elsevier Inc. All rights reserved.
http://dx.doi.org/10.1016/j.neuroimage.2013.11.047

point, the global network dynamics reveals correlation patterns that are spatially shaped by the underlying anatomical structure, leading to an optimal fit with the empirical BOLD functional connectivity. However, the relationship with the faster oscillatory rhythms typically observed with electroencephalography (EEG) and magnetoencephalography (MEG) in the resting-state has only briefly been addressed in computational models (Cabral et al., 2011; Deco et al., 2009; Ghosh et al., 2008b).

From the experimental side, several studies have aimed to investigate the neurophysiological counterpart of resting-state BOLD signal fluctuations using simultaneous fMRI and intra-cranial recordings (Nir et al., 2008; Shmuel and Leopold, 2008), simultaneous fMRI and EEG (de Munck et al., 2007; Difrancesco et al., 2008; Goldman et al., 2002; Laufs et al., 2003b; Mantini et al., 2007; Ritter et al., 2009) and, more recently MEG (Brookes et al., 2011b; de Pasquale et al., 2010; Hipp et al., 2012; Liu et al., 2010; Nikouline et al., 2001). Taken overall, results indicate that resting-state BOLD signal fluctuations are driven by slow modulations in the power (or the amplitude) of brain oscillations in a certain frequency range (note that the average power of an oscillation in a given time window is proportional to its squared amplitude). However, different frequencies show distinct correlation behaviors with BOLD signal fluctuations. On one side, intra-cranial recordings report that the BOLD signal displays a *positive* correlation with the firing rate and/or power of gamma-frequency oscillations (40–100 Hz) in the recording site. On the other side, studies using simultaneous recordings of EEG-fMRI point to an inverse correlation between the BOLD signal and the power of alpha (8–13 Hz) and beta (13–30 Hz) oscillations indicating that the so-called "idle rhythms" may be associated with deactivation and decreased metabolic rate. Moreover, recent MEG studies of resting-state activity have found slow fluctuations in the power (or amplitude) of neural oscillations that correlate across distant brain areas, especially when considering 8–30 Hz oscillations—the typical frequency range of alpha and beta rhythms (Brookes et al., 2011b; de Pasquale et al., 2010; Hipp et al., 2012; Liu et al., 2010; Luckhoo et al., 2012; Nikouline et al., 2001). Notably, these amplitude modulations yield large-scale functional networks that correspond quantitatively to the resting-state networks derived from rs-fMRI (Brookes et al., 2011b). In general, these reports indicate that resting-state functional connectivity in BOLD responses corresponds to a spatially structured amplitude modulation of neural oscillations in the 8–30 Hz range. However, the mechanism at the genesis of these structured frequency-specific amplitude fluctuations remains unknown.

In the present work, we aim to investigate the source of structured amplitude fluctuations observed in MEG signals at rest. We use a whole-brain network model of spontaneous activity, previously introduced in Cabral et al. (2011) to model spontaneous BOLD functional connectivity. The model consists in a variant of the Kuramoto model of coupled oscillators adapted to incorporate the spatial and temporal characteristics of the structural connectome. In other words, the coupling strength between each pair of oscillators is scaled by the number of white-matter fibre tracts detected between the corresponding brain areas and the time-delays are proportional to the structural distance between them (Cabral et al., 2011; Kuramoto, 1984; Yeung and Strogatz, 1999). In our previous research (Cabral et al., 2011), we found that the optimal fit with resting-state BOLD functional connectivity occurred for a critical range of model parameters where the system exhibited slow spontaneous fluctuations in the synchrony degree of sub-groups of brain areas (or clusters), leading to structured BOLD signal fluctuations. Here, we hypothesize that these fluctuations in the synchrony degree may also modulate the oscillators' frequency, leading to frequency-specific amplitude fluctuations, making the link between fMRI and MEG expressions of resting-state activity. This hypothesis is supported by findings in the literature of the Kuramoto model showing that the synchronization of coupled oscillators with time-delays induces a suppression of the oscillators' natural frequency (Niebur et al., 1991). Although these findings refer to simpler network structures, they are helpful to depict the synchronization phenomena occurring in complex coupled systems like the brain (Breakspear et al., 2010).

Methods

MEG data collection and analysis

Ten normal healthy participants (3 males, 20–39 years old, mean 27.9) underwent an eyes-closed resting-state MEG scan lasting 5 min on an Elekta Neuromag Vectorview system (Elekta Neuromag Oy, Helsinki, Finland). Data were collected on 102 magnetometers and 102 pairs of orthogonal planar gradiometers at 1000 Hz sampling frequency. Head localization was achieved using four head position indicator (HPI) coils. The HPI coils were continuously energized throughout the scan but movement compensation was not performed — instead the initial head position was used for co-registration. Each subject's head shape was recorded using a Polhemus Isotrack system. Structural MRIs were gathered on a Siemens 3 T MR scanner with a resolution of 1x1x1 mm.

Signal space separation (implemented using MaxFilter™) was applied to each data-set to reduce interference from outside the scanner helmet (Taulu et al., 2005). The sensor space MEG data were de-noised using temporal independent component analysis (ICA) to remove cardiac, 50Hz mains and, in some subjects, eye movement artifacts. The MEG data were then visually inspected and any channels with high variance or obvious artifacts were excluded. Epochs of variable length that contained high variance and transient spikes in gamma power were flagged as bad. Bad epochs were excluded from critical stages (such as covariance estimation) but included in stages where data continuity was required (such as the Hilbert transform).

Each dataset was then co-registered into the Montreal Neurological Institute (MNI) space by registering the canonical MNI template to the Polhemus head shape data. An overlapping-spheres forward model was implemented using a quasi-static approximation of Maxwell's equations onto a simplified geometric model of the head—in this case the head is modeled using a basis set of spherical harmonic volumes (Huang et al., 1999). Both co-registration and forward model estimation were performed with the Matlab SPM8 package (www.fil.ion.ucl.ac.uk/spm). The data were band-pass filtered into 10 frequency bands: 2–6 Hz; 4–8 Hz; 6–10.5 Hz; 8–13 Hz; 10.5–21.5 Hz; 13–30 Hz; 21.5–39 Hz; 30–48 Hz; 39–66 Hz and 52–80 Hz. In this selection of frequency bands we include typical human brain rhythms such as the alpha (8–13 Hz), beta (13–30 Hz) and gamma (low: 30–48 Hz, high: 52–80 Hz) rhythms. A LCMV beamformer (Robinson and Vrba, 1998; Van Veen et al., 1997; Woolrich et al., 2011) was used to transform the original sensor time series for each frequency band into source space time series, that is, to reconstruct the activity at the center locations of 90 brain regions defined by the AAL brain parcellation template (Tzourio-Mazoyer et al., 2002) (see Fig. 1 for an illustration).

The beamformer outputs 90 time-series for each of the 10 frequency-bands of interest. Recent studies have shown that spontaneous functional connectivity in MEG data is best captured by considering the correlations between low-frequency amplitude envelope fluctuations of the band-limited source space estimates of neural activity at each location (Brookes et al., 2011a, 2011b; de Pasquale et al., 2010, 2012; Liu et al., 2010; Luckhoo et al., 2012). To obtain the envelopes, we computed the modulus of the *analytic signal* at each node using the Hilbert transform. In more detail, the analytic signal $R_n(t)$ is a complex number given as:

$$R_n(t) = X_n(t) + iH_n(t),$$

whose real part $X_n(t)$ is the time course estimated at each of the $n = 1,\ldots,90$ source locations and the imaginary part $H_n(t)$ is the Hilbert transform of the time courses. The analytic signal is a complex-

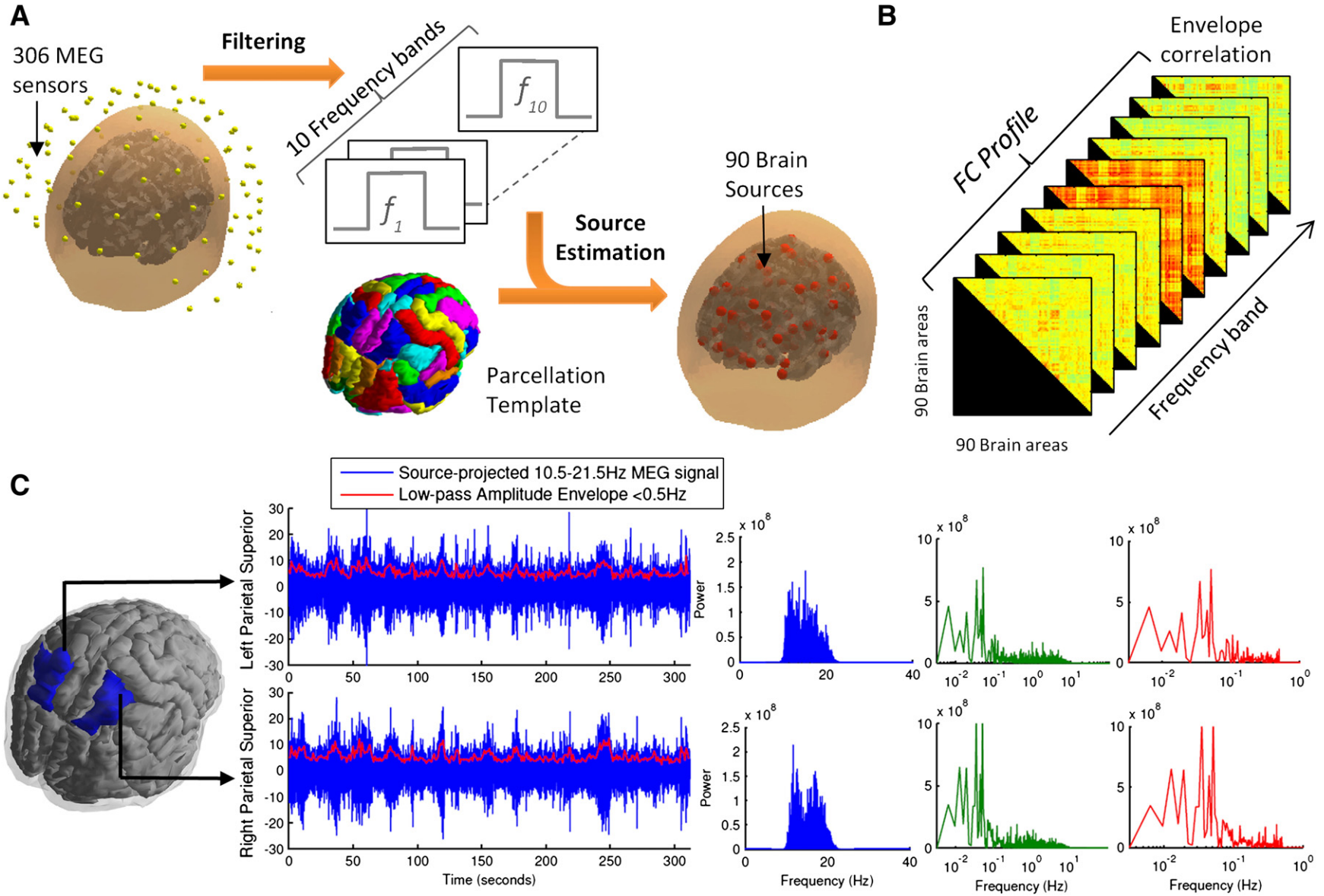

Fig. 1. MEG data collection and analysis. (A) The signals detected at the MEG sensors were filtered into 10 frequency bands (f = [2–6 Hz]; [4–8 Hz]; [6–10.5 Hz]; [8–13 Hz]; [10.5–21.5 Hz]; [13–30 Hz]; [21.5–39 Hz]; [30–48 Hz]; [39–66 Hz] and [52–80 Hz]). For each frequency band, the activity was estimated at 90 sources located at the center of the brain regions defined in the AAL parcellation template (see Table S1 for the list of brain areas). (B) For each frequency band, we computed the correlation matrix between the envelopes of the 90 source-reconstructed signals. The functional connectivity (FC) profile was obtained by collating the values in the upper triangular part of the matrices. The FC profiles were averaged across 10 healthy subjects at rest. (C) The MEG signal estimated in two brain areas (left and right superior parietal) in the 10.5–21.5 Hz frequency band (blue) and the corresponding amplitude envelope low-pass filtered with a cut-off frequency of 0.5Hz (red). The plots on the right side show the power spectra of the source-reconstructed signals (blue), the unfiltered envelopes (green) and the low-pass filtered envelopes (red).

valued quantity that can be expressed in polar form using Euler's formula as:

$$R_n(t) = A_n(t)e^{i\psi(t)}$$

where $A_n(t)$ is the amplitude – or *envelope* – of the analytic signal and $\psi_n(t)$ is the phase of the analytic signal.

For each pair of AAL nodes, prior to envelope estimation, the node time courses were orthogonalized to remove all zero-lag correlations. This is because MEG functional connectivity between two regions has a spurious contribution due to signal leakage between the two regions. This signal leakage is zero-lag and so is removed by orthogonalizing the time series (Brookes et al., 2012; Hipp et al., 2012). Any subsequent correlations measured in the envelopes of the orthogonalized nodes cannot be due to signal leakage.

The low-frequency component of the envelope fluctuations have been found to be optimal for measuring spontaneous MEG functional connectivity (Brookes et al., 2011a, 2011b; Hipp et al., 2012; Liu et al., 2010; Luckhoo et al., 2012). As such, envelopes were low-pass filtered using a cut-off frequency of 0.5Hz before estimating correlations. As shown in Fig. 1C, we find that the envelope fluctuations are intrinsically slow, peaking below 0.1Hz, and therefore the main component of the signal is maintained when low-pass filtering the envelopes below 0.5Hz.

For each subject, we obtain a total of 10 frequency-specific zero-lag corrected envelope correlation matrices, or functional connectivity (FC) matrices. The FC matrices were averaged across the 10 subjects to give a single set of 10 FC matrices (shown in Fig. 3E).

Structural brain networks

The structural brain networks used in the model were estimated from diffusion tensor imaging (DTI) data using a modified version of already published methods (Gong et al., 2009) (see Fig. 2). The data was obtained from 21 healthy, normal participants (11 males and 10 females, age: 22–45 years) different from the 10 healthy subjects from which MEG data was recorded. All scans were performed on the same Philips Achieve 1.5 Tesla Magnet. Diffusion MRI was acquired by using a single-shot echo planar imaging-based sequence with coverage of the whole brain with 33 optimal nonlinear diffusion gradient directions ($b = 1200$ s/mm^2) and 1 non-diffusion weighted volume ($b = 0$), repetition time (TR) = 9390 ms; echo time (TE) = 65 ms. Twelve healthy participants used a reconstructed matrix of 128 × 128 and reconstructed voxel size 2.5 × 2.5 × 2.5 mm^3. Nine healthy participants used a reconstructed matrix of 176 × 176 and reconstructed voxel size of 1.8 × 1.8 × 2 mm^3. We also acquired T1-weighted structural images with a three-dimensional 'FLASH' sequence (TR = 12 ms, TE = 5.6 ms, flip angle = 19°, with elliptical sampling of k-space, giving a voxel size of 1 × 1 × 1 mm in 5.05 min).

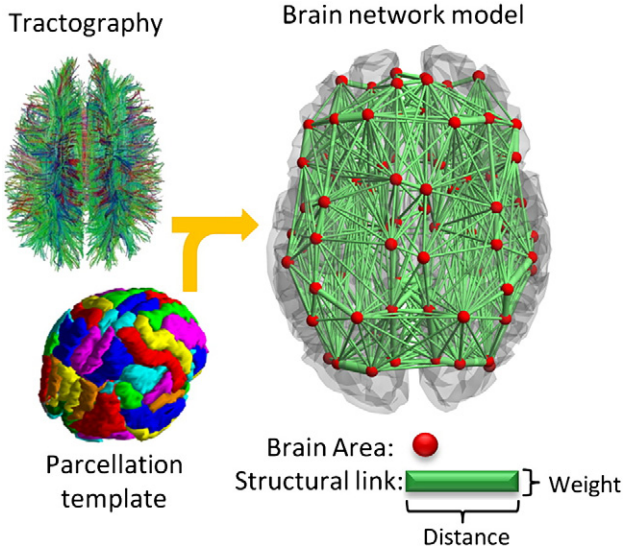

Fig. 2. The spatiotemporal structure of the brain network. Interactions between brain areas are mediated by myelinated axonal fibers, which can be detected with tractography from diffusion tensor images. Since regions are spatially segregated and the transmission speed is finite, interactions are time-delayed. In our model, each node represents a brain area. Links are weighted in proportion to the number of white matter fibre tracts detected and time delays are scaled by the distance between areas.

The AAL template was used to parcellate the brain into 90 regions (45 for each hemisphere) to define the network nodes. For each participant, parcellation was conducted in the diffusion-MRI native space. The b0 image in diffusion-MRI space was linearly co-registered to the T1-weighted structural image using the Flirt tool (FMRIB, Oxford) (Jenkinson et al., 2002). The transformed T1-weighted image was then mapped to the T1 template of ICBM152 in MNI space (Collins et al., 1994), inversed and further applied to warp the AAL mask from MNI space to the diffusion-MRI native space. Interpolation using nearest-neighbor method ensured the preservation of labeling values.

The links between nodes were weighted in proportion to the number of white matter tracts detected between brain areas. The processing of the diffusion-MRI data was performed using the Fdt toolbox in FSL (www.fmrib.ox.ac.uk/fsl, FMRIB). Pre-processing involved the co-registration of the diffusion-weighted images to a reference volume using an affine transformation for the correction of head motion as well as eddy current induced image distortion. Subsequently, the local probability distribution of fiber direction at each voxel was estimated (Behrens et al., 2003). We then used the probtrackx algorithm allowing for automatic estimation of two fiber directions within each voxel, which can significantly improve the tracking sensitivity of non-dominant fibre populations in the human brain (Behrens et al., 2007).

For each voxel in the brain, we applied probabilistic tractography to sample 5000 streamline fibers passing through that voxel. The connectivity probability from voxel i to another voxel j was defined by the proportion of fibers passing through voxel i that reach voxel j (Behrens et al., 2007). This was then extended from the voxel level to the region level. The connectivity C_{np} from region n to region p is calculated as the number of fibers passing through any voxel in region n that connect to any voxel in region p, divided by 5000*N, where N is the number of voxels in region n. For each brain region, the connectivity to each of the other 89 regions was calculated. Since the connectivity from n to p is not necessarily equal to that from p to n but highly correlated for all subjects (the least Pearson $r = 0.70$, $p < 10^{-50}$), we defined the undirectional connectivity C_{np} between regions n and p by averaging the two. We implemented the calculation of regional connectivity using in-house Perl scripts.

Model of coupled oscillators with time-delays

To explore the spontaneous behavior of coupled brain areas, we used a variant of the original Kuramoto model, which describes the dynamics of coupled oscillators systems (Acebron et al., 2005; Kuramoto, 1984). Different variants of the Kuramoto model have been used to simulate synchronization phenomena in biological systems (Pikovsky et al., 2001; Strogatz, 2003) and, more recently, neural dynamics (Breakspear et al., 2010; Cabral et al., 2011; Kitzbichler et al., 2009; Yan and Li, 2013). Reducing the dynamics of a brain region to a phase-oscillator involves a high degree of abstraction. This approach is supported by a number of experimental and theoretical studies showing that neural activity at the population level usually exhibits oscillations with a moderate level of synchrony, in particular in the gamma frequency range (30–80 Hz) (Bartos et al., 2007; Borgers and Kopell, 2003; Brunel, 2000; Brunel and Wang, 2003). Such self-sustained oscillations are due to a balance

in the firing rates of excitatory and inhibitory neurons in a neural population. In this framework, the firing rates describe a closed periodic trajectory in phase space—called a limit cycle, and the dynamics can be approximated by a single dynamical variable, which is the angle – or phase – on this cycle. Therefore, the resulting node model is a phase-oscillator and the whole system is a network of coupled phase-oscillators.

A crucial step toward neurobiological plausibility of the model is the introduction of time delays between coupled brain regions. Time delays arise from finite axonal transmission times, which depend on the inter-areal distance and on the myelination level of the fibre tracts, as well as from synaptic and dendritic time constants. Time delays are known to affect the dynamics of coupled oscillators, especially when they are in the same order of magnitude as the oscillation period (Baldi and Atiya, 1994; Dhamala et al., 2004; Ghosh et al., 2008a; Jirsa, 2009; Knock et al., 2009). For this reason, it is important to consider time-delays in large-scale brain models where the local nodes display – either damped or self-sustained – oscillations (Cabral et al., 2011; Deco et al., 2009; Ghosh et al., 2008b).

The influence that one node exerts on another is written as a sine function of the delayed phase difference between the two oscillators (Yeung and Strogatz, 1999). Denoting by $\theta_n(t)$ the phase of node n at time t, it then obeys the following dynamical equation:

$$\frac{d\theta_n}{dt} = \omega + k\sum_{p=1}^{N} C_{np}\sin\left(\theta_p\left(t-\tau_{np}\right)-\theta_n(t)\right), n = 1,\ldots,N$$

This equation differs from the classic Kuramoto model in that the natural frequency is identical for all oscillators $\omega_n = \omega, \forall n \in N$, the coupling is heterogeneous and the phase relationships are time-delayed. The natural frequency was assumed to be $\omega = 2\pi \times 40Hz$, the same frequency displayed by the Wilson–Cowan units used in the network model of Deco et al. (2009). Note that a distribution of natural frequencies does not alter the results of this work (see Figure S2). C_{np} is the coupling strength from node p to node n, which is proportional to the number of fibre tracts detected between the two nodes (see Section 2.3) and normalized so that $\overline{C} = 1$. k is the global coupling weight that uniformly scales all connection weights. The delay $\tau_{np} = D_{np}/v$ is proportional to the Euclidean distance D_{np} between the centers of gravity of the AAL brain areas and to the conduction velocity v in myelinated fibers (which, again for simplicity, we assumed to be homogeneous (Deco et al., 2009; Ghosh et al., 2008a)). Since the coupling weights C_{np} and the distances D_{np} between nodes are fixed, the only two free parameters in the model are the global coupling weight k and the conduction velocity v. By increasing or decreasing v, the delays become shorter or longer, shifting the mean of the delay distribution $\overline{\tau}$. To get a better insight on the effect of delays in the system, we performed simulations as a function of the *mean* of the delay distribution, $\overline{\tau}$ - which is equivalent to varying v since the distances between nodes are fixed.

The system of N coupled delay differential equations was numerically integrated using an Euler scheme (with a sufficiently small time-step of $\Delta t = 0.1$ ms). Note that no noise was added to the system, and therefore the simulated signals are deterministic. The only randomness introduced in the system was on the phases at $t = 0$ (initialized randomly in each simulation). Note that the main results of the model are independent of the initial conditions (data not shown). To define the initial history (necessary due to the delays), phases were estimated for a sufficiently large initial period in a non-interacting way. Simulations were run for 300 s for a range of parameters k and $\overline{\tau}$, removing the first 20s of simulations to discard the transient dynamics. The neural activity $r_n(t)$ at each of the 90 brain regions oscillates around a fixed value, and these oscillations are given by a periodic function f of the phase at each node n, $r_n(t) = f(\theta_n(t))$. Following the assumption made in Cabral et al. (2011), we used the sine function to transform the phases into neural activity $r_n(t) = r_0\sin(\theta_n(t))$ and considered a constant amplitude $r_0 = 1$.

For each set of parameters k and $\overline{\tau}$, the simulated neural activity was compared with empirical data (see Section 2.5). Selecting the set of parameters k and $\overline{\tau}$ that provided the best fit with experimental data, the model was rerun for 1200 s (20 minutes). All calculations were performed using a commercial software package (MATLAB 7.12, The MathWorks Inc., Natick, MA, 2011).

At the global level, the network synchrony was evaluated by the order parameter $R(t)$ defined by:

$$R(t)e^{i\Phi(t)} = \frac{1}{N}\sum_{n=1}^{N} e^{i\theta_n(t)},$$

where $R(t)$ measures phase uniformity, varying between 1 for a fully synchronized state and 0 for a fully incoherent state. $\Phi(t)$ describes the phase of the global ensemble. To characterize the system's synchronization behavior in the parameter space of k and $\overline{\tau}$, we estimated the mean synchrony level, $\overline{R}$, and the standard deviation, σ_R, which captures how the synchrony degree fluctuates in time. Fluctuations in the synchrony degree have been associated with the existence of metastable synchronized states and therefore σ_R is indicative of the system's *metastability* level (Shanahan, 2010; Wildie and Shanahan, 2012).

The simulated time-series $r_n(t)$ were band-pass filtered into the same 10 frequency bands used to filter the MEG data. Subsequently, the amplitude envelopes were estimated via the Hilbert transform as the modulus of the analytic signals. These envelopes were low-pass filtered with a cut-off frequency at 0.5Hz as in the real MEG data. The FC matrices were obtained by computing the envelope correlation matrices (unlike the real MEG data, there is no signal leakage in the simulations and therefore the simulated signals were not orthogonalized).

Comparison between experimental data and numerical simulation

The values on the upper triangular part of the FC matrices (see Fig. 1B) were collated over the 10 frequency bands to obtain a vector (with 10*N*(N-1)/2 values) representing the *FC profile* (since the matrices are symmetric, in this way we ensure to consider only unique entries and exclude the diagonal values). The FC profile was estimated in the same way from the real MEG FC matrices and the simulated FC matrices. The model's performance was evaluated by computing the Pearson's correlation coefficient (ρ) between the real MEG FC profile and the simulated FC profile obtained for each set of parameters k and $\overline{\tau}$.

Results

Frequency-specific envelope functional connectivity

The FC profiles obtained from simulations were compared with the real MEG FC profile for a range of model parameters. As can be observed in Fig. 3A, the fit between real and simulated FC profiles (see Section 2.4) is sensitive to the global coupling weight k and the mean of the delay distribution $\overline{\tau}$. The model shows the best agreement with experimental data for a limited range of global parameters (area indicated within dashed ellipse) reaching correlations up to $\rho = 0.41$ between empirical and simulated FC profiles, which is noteworthy given the high level of abstraction and simplicity of the model. The synchronization behavior of the system is shown for the same range of parameters in Fig. 3B–C. In the range of best agreement with empirical MEG data, the average synchrony degree of the system is moderate ($0.3 < \overline{R} < 0.4$), indicating that it is neither fully synchronized ($\overline{R}$ close to 1), neither incoherent ($\overline{R}$ close to 0). Importantly, in this range of parameters the synchrony degree exhibits fluctuations over time ($0.1 < \sigma_R < 0.2$). Moreover, as shown in Fig. 3D, the envelopes of 8-30Hz oscillations display high fluctuations in this region of parameters (In Section 3.2 we investigate the origin of these fluctuations).

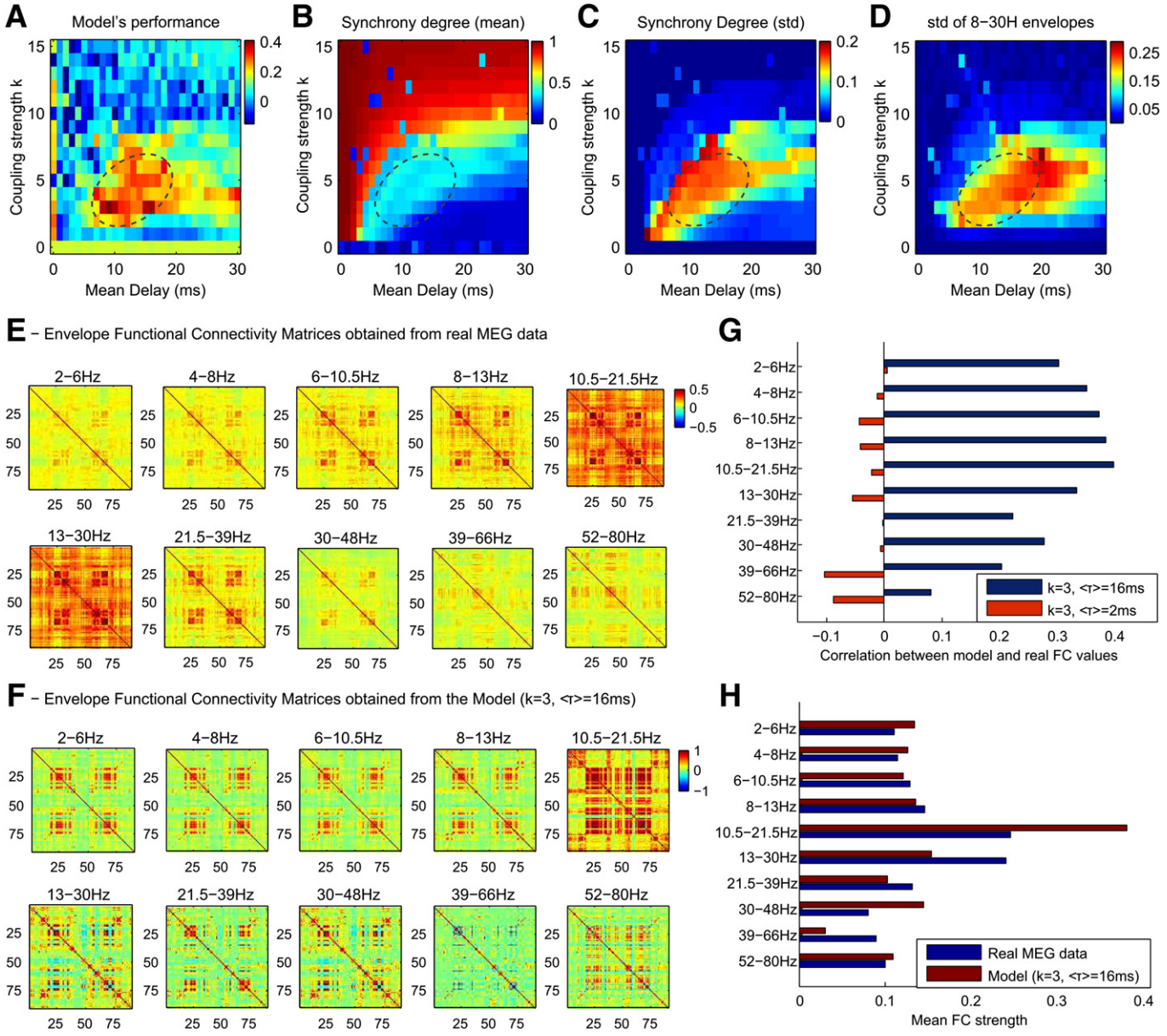

Fig. 3. Simulated envelope functional connectivity. (A) Correlation between the real and simulated FC profiles as a function of the coupling strength and the mean of the delay distribution. The area within the dashed line indicates the parameter range for which the model best estimates real MEG FC profiles. (B) Mean synchrony degree (1 = full synchrony; 0 = incoherence) for the same range of model parameters. The system exhibits a high degree of synchrony when the delays are small (mean < 3 ms). For larger delays, synchrony is possible with an increased coupling strength. Note that, when k = 0 (bottom line), the oscillators are uncoupled. (C) Fluctuations in the synchrony degree are indicative of a metastable synchronization regime. For sufficiently large delays, metastable synchronization occurs in the border between incoherence and full synchrony. The best agreement with experimental data (dashed line) was obtained in this regime. (D) In the presence of time-delays, the metastable synchronization induces a modulation of the oscillators' frequency. This generates envelope fluctuations of 8–30 Hz oscillations. (E–F) Set of frequency-specific envelope functional connectivity matrices obtained from resting MEG data (E) and from the model (F). (G) Correlation between the real and simulated matrices as a function of the frequency, for two parameter sets: one where a good agreement with MEG data was found (blue), and another with shorter delays, for which the model failed (red). (E) Mean functional connectivity (estimated as the average correlation strength between envelopes) as a function of the frequency band.

In Fig. 3E and F we show the envelope correlation matrices for each frequency band of the real MEG data and the simulated data obtained at $k = 3$ and $\overline{\tau} = 16$ ms (where the model showed the best agreement with experiments). In Fig. 3G, the FC profiles of real and modeled data were compared separately for each of the 10 frequency bands. Results are shown for the optimal working point ($k = 3, \overline{\tau} = 16$ ms) and for another simulated dataset where the coupling strength was maintained ($k = 3$) but the speed of transmission was increased, shifting the mean of the delay distribution down to $\overline{\tau} = 2$ ms. For the optimal working point, the simulated FC shows a good agreement with the empirical FC for all frequency bands ($\rho = 0.30 \pm 0.09$, mean ± standard deviation). On the other hand, when the delays are too short, the model fails to reproduce the empirical data and the mean correlation with the real FC profiles is reduced to $\rho = -0.04 \pm 0.04$. This example illustrates the key role of time-delays in the model in shaping the frequency-specific FC profiles.

In Fig. 3H we calculate the average functional connectivity between envelopes as a function of the frequency range used to bandpass the MEG signals (or *carrier frequency band*). In the real MEG data, we find that the functional correlations are stronger for carrier

frequency bands in the 8-30Hz range (the typical range of alpha- and beta-frequency oscillations), peaking for the 10.5–21.5 Hz band, corroborating previous resting-state MEG studies reporting frequency-dependent functional connectivity during rest with a peak in the low-beta frequency range (Brookes et al., 2011a, 2011b; de Pasquale et al., 2010, 2012; Hipp et al., 2012; Luckhoo et al., 2012). Subsequently, the same analysis was performed on the simulated data obtained at the optimal working point. The plot show that the data obtained with the model exhibits a frequency-specificity similar to the one observed experimentally, displaying stronger FC in the envelopes of 10.5–21.5 Hz oscillations, a frequency much slower than the natural frequency of the oscillators (f = 40Hz). These correlated amplitude fluctuations of oscillations slower than the natural frequency occur due to the delayed phase interactions occurring in the space-time structure of the network (see Section 3.2).

To explore how well the model estimates the FC at the regional level, we computed the correlation between the envelopes of a given region (the seed) with all other brain areas, for different frequency bands. The resulting correlation patterns can be interpreted as seed-based functional connectivity maps. The anatomical connectivity and the empirical and simulated functional connectivity at 3 frequency bands (8 to 13 Hz, 10.5 to 21.5 Hz and 39 to 66 Hz) is reported in Fig. 4 for two seeds: the left Superior Parietal and the left Superior Motor Area (in Fig. S1 we show examples with other seeds and frequencies). We observe that structurally connected brain areas are likely to be functionally connected. However, the opposite is not true, and many brain areas appear functionally connected although no white-matter tract has been detected between. However, despite the missing structural links, we find that the model is able to reproduce some long-distance inter-hemispheric functional connections that are not mediated by any direct structural link, possibly mediated by intermediate connections.

Origin of envelope correlations

In the model, structured envelopes of band-pass filtered signals similar to the ones observed in real MEG data emerge spontaneously from time-delayed network interactions between gamma-band oscillators. However, how these structured envelopes are generated is not straightforward. The main advantage of using a simple model of coupled oscillators with respect to more realistic models is that the synchronization phenomena occurring in the system can be analyzed in the light of the existing literature on coupled oscillators. Although the networks addressed in analytic studies are far less complex than the brain network, they allow for a depiction of the physical mechanisms at the genesis of the envelope fluctuations observed in the model.

As shown in Fig. 3B–D, the envelopes of 8–30Hz oscillations exhibit fluctuations for a range of parameters that fall in the critical boundary between incoherence and synchrony. In this border regime, the synchrony degree fluctuates in time (Fig. 3C). Wildie and Shanahan (2012) have shown that such fluctuations in the synchrony degree are due to a metastable synchronization regime, where a number of "chimera" states – characterized by coexistent synchronized and desynchronized subsystems – are formed. In other words, intermittent synchronization occurs between subsets of nodes, forming metastable coalitions. However, how this metastable regime generates oscillations different from the natural frequency of the oscillators (40 Hz) remains unanswered. To understand this phenomenon, one needs to consider the work from Niebur et al. (1991), who analyzed the synchronization frequency of coupled oscillators with time-delayed nearest-neighbor coupling. They report that "*even small delay times lead to a novel form of frequency depression where the system decays to stable states which oscillate at a delay and interaction-dependent reduced collective frequency*" (Niebur et al., 1991). Combining this finding with the metastable regime described before, one can hypothesize that when oscillators are in a metastable synchronized state, their oscillation frequency is temporarily slowed down. In this way, a system of coupled oscillators with time-delays in the metastable regime may display spontaneous *frequency modulation*.

In Fig. 5A, the simulated signal $r_n(t) = \sin(\theta_n(t))$ is plotted for 2 seeds: the left and right superior parietal areas. The signals are uncorrelated ($\rho = 0.06$) and have constant amplitude (i.e. $-1 \leq \sin(x) \leq 1$). If the signals are modulated in frequency due to metastable synchronization (as hypothesized) then, when the signals are band-pass filtered in the range of the reduced collective frequency, they should exhibit *correlated amplitude fluctuations*. Fig. 5B shows the simulated signals band-pass filtered in two frequency bands: 10.5-21.5Hz (the frequency at which higher envelope functional connectivity was observed in both real and simulated data) and 30-48Hz (which includes the natural frequency of the oscillators in the model $f = 40Hz$). The band-passed signals, unlike the unfiltered signals, display amplitude fluctuations. Importantly, the envelopes at 10.5-21.5Hz are highly correlated ($\rho = 0.79$) between the two nodes, indicating that the two nodes belong to a subsystem whose reduced collective frequency is in this frequency range. On the other hand, the envelopes in the 30-48Hz range are uncorrelated ($\rho = 0.03$). Observing the envelope of the signal in the 10.5-21.5Hz range on a larger temporal window (Fig. 5C left), it can be seen that it fluctuates on a very slow time scale, with a peak below 0.1Hz (Fig. 5C right). This time-scale of envelope fluctuations is in the same range as the one found in the real MEG data (as shown in Fig. 1C).

To investigate the origin of the envelope fluctuations of the band-pass filtered signals, we plot the spectrogram – i.e. frequency versus time - of the *unfiltered* simulated signal in the same brain area (Fig. 5D). In this plot, temporary increases in the power around 16Hz can be observed, lasting sometimes for several seconds. For each time window and for each frequency bin, the power P is given by $P = (A^2)/2$, where A is the amplitude of the signal. As such, when the signal is band-pass filtered around 16Hz, it displays amplitude fluctuations that directly express the power fluctuations around 16Hz observed in the spectrogram. Furthermore, and corroborating our previous hypothesis, those increases in the power around 16Hz appear directly associated with periods of increased synchronization in the system (Fig. 5E). Indeed, the synchrony degree of the system (estimated using the Kuramoto order parameter) is strongly correlated with the envelopes of 10.5-21.5Hz oscillations ($\rho = 0.53$ and $\rho = 0.48$ for the left and right superior parietal). Notably, if only the slow part (<0.5Hz) of the envelopes (and order parameter) is considered, the correlations are further increased ($\rho = 0.95$ and $\rho = 0.92$ for the left and right superior parietal). These results demonstrate that the envelope fluctuations of band-pass filtered signals observed in the model are caused by slow fluctuations in the synchrony degree due to the spontaneous formation and dissolution of metastable chimera states. This mechanism leads to spatially structured frequency specific power fluctuations, which, according to our model results, fairly reproduce spontaneous MEG functional connectivity.

To investigate how much of the brain's space-time structure is responsible for the observed phenomena, we reran the model changing different features of the coupling matrix and the distance matrix (Fig. 6). In particular we tested the model using a randomized coupling matrix with conserved degree distribution and connectedness (Maslov and Sneppen, 2002; Rubinov and Sporns, 2010), homogeneous coupling weights ($C_{np} = 1, \forall C_{np} > 0$) or homogeneous distances ($D_{np} = \overline{D}, \forall n, p \forall N$). Randomizing the connectivity matrix (but keeping exactly the same coupling weights and the same distances) not only destroys the fit with the empirical functional connectivity but also leads to a total disruption of the metastable dynamics. This indicates that the connection topology, i.e. the way brain areas are connected to each other in a non-random way, is a key ingredient to obtain metastable chimera states in systems of delayed coupled oscillators (Wildie and Shanahan, 2012). Furthermore, we found that the use of homogeneous coupling weights or homogeneous delays significantly reduces the

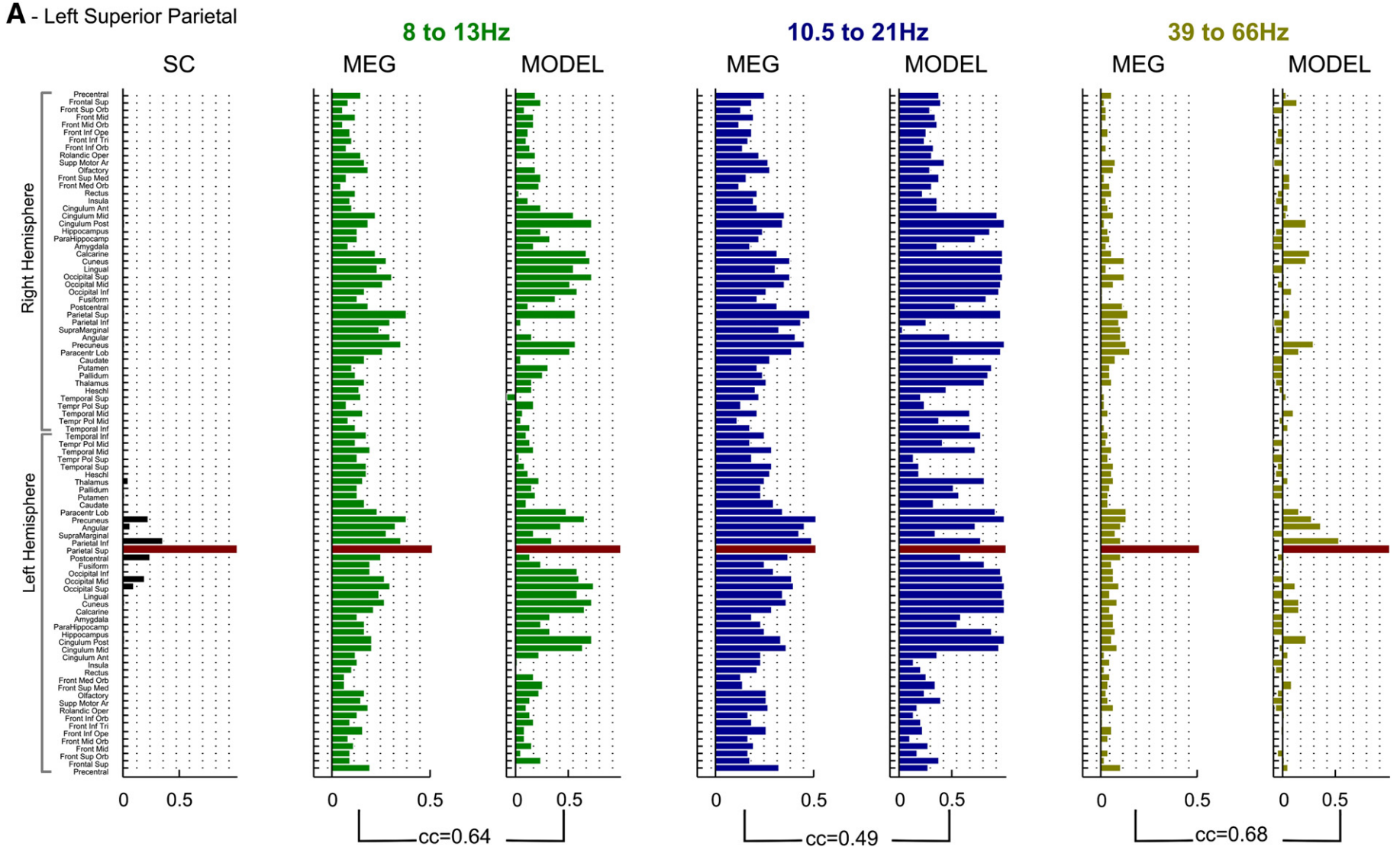

Fig. 4. Real and simulated connectivity of 2 seeds. Horizontal bars indicate the connectivity (structural/functional real/simulated) of the left Superior Parietal Area (top) and the left Superior Motor Area (bottom) with all other brain areas. The line corresponding to the seed is marked in dark red. The structural connectivity, obtained from tractography, is reported black. Green, blue and yellow bars indicate the real (left) and modeled (right) envelope correlation for 8–13 Hz, 10.5–21.5 Hz and 39–66 Hz frequency bands, respectively.

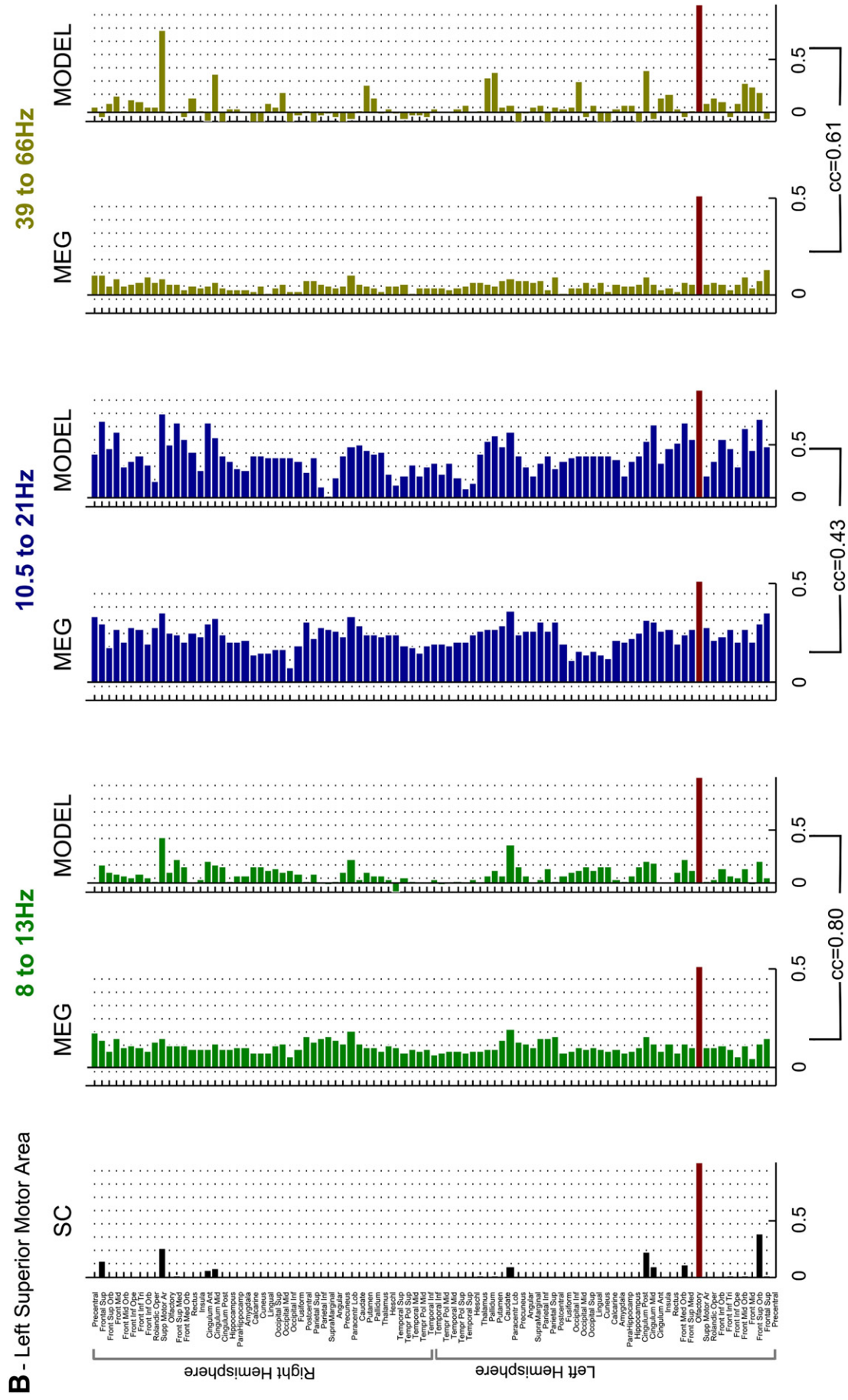

Fig. 4 (*continued*).

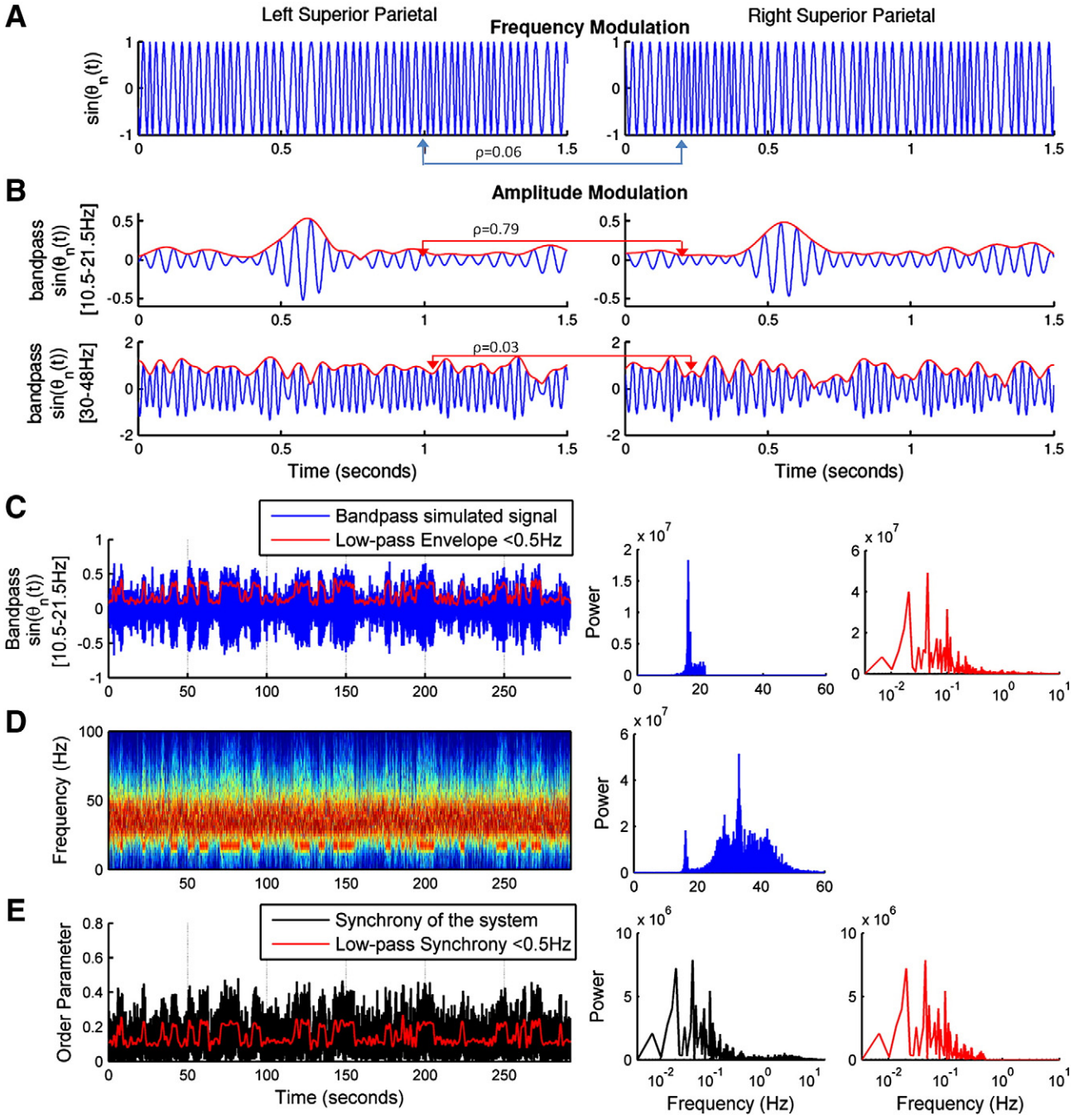

Fig. 5. Slow and structured envelope fluctuations emerge from metastable synchronization regime. (A) Simulated signal $r_n(t) = \sin(\theta_n(t))$ in the left and right Superior Parietal areas. The two signals are uncorrelated ($\rho = 0.06$ for a 1200 s simulation period). (B) Same signals bandpass filtered in 2 frequency bands: 10.5 to 21.5 Hz and 30 to 48 Hz. The signals band-passed at 10.5–21.5 Hz display correlated envelopes ($\rho = 0.79$), whereas the envelopes of the signals band-passed at 30–48 Hz are uncorrelated ($\rho = 0.03$). As in (A), correlations were estimated for the whole simulation period. (C) (Left) Simulated signal on the Left Superior Parietal Area band-pass filtered between 10.5 and 21.5 Hz (same as in B-top-left, but for a longer time window). The amplitude envelope fluctuates on a very slow time scale. (Middle) Power spectrum of the band-pass filtered signal, with a peak at 16Hz. (Right) Power spectrum of the (unfiltered) amplitude envelope, showing a peak below 0.1 Hz. (D) Spectrogram showing the instantaneous frequency of the (unfiltered) simulated signal $r_n(t) = \sin(\theta_n(t))$ on the left Superior Parietal Area (left) and the corresponding time averaged power spectral density function (right). Although most of the power is contained in the 25–50 Hz range, we find intermittent increases in the power around 16 Hz, indicating that oscillations in that frequency range may emerge for periods of several seconds and then disappear. These intermittent increases in the power are intrinsically related to the amplitude fluctuations of band-pass filtered signals observed in (C). (E) Synchrony degree of the system estimated using the Kuramoto order parameter. Due to the metastable synchronization regime, periods of higher synchrony (lasting for several seconds) alternate with periods of lower synchrony. The synchrony degree is strongly correlated with the envelope of 10.5–21.5 Hz oscillations ($\rho = 0.53$) showing that the modulation in the power (and amplitude) of band-pass filtered oscillations is due to the metastable synchronization regime. Moreover, if only the slow part (<0.5 Hz) of the envelope (and order parameter) is considered, the correlation is higher ($\rho = 0.95$), indicating that the emergence of reduced collective frequencies occurs only when the synchronization is sufficiently long.

range of parameters where a metastable regime is obtained. These results show that the space–time structure of couplings and delays in the human brain provides an optimal network structure to support a robust metastable dynamics in which different subsystems may temporarily synchronize, while the global system never fully synchronizes.

Discussion

In this study, we have combined experimental and theoretical work to investigate the mechanisms of spontaneous MEG functional connectivity. From the MEG data of 10 healthy participants at rest we found

that the amplitude envelopes of band-pass filtered signals fluctuate on a slow time-scale (<0.1 Hz) and exhibit higher correlations – or functional connectivity – for oscillations in the 8-30Hz range (peaking in the 10.5–21.5 Hz frequency band) corroborating previous experimental observations of frequency-specific envelope functional connectivity in MEG data (Brookes et al., 2011b; de Pasquale et al., 2010, 2012; Hipp et al., 2012; Liu et al., 2010; Nikouline et al., 2001).

Using a simple model of coupled oscillators with time delays, we have shown how slow and structured amplitude envelopes of band-pass filtered signals may be generated in the space-time structure of the brain. Unlike more detailed models of spontaneous activity – which simulate more realistic but sometimes less interpretable data – the model employed allows to interpret the simulation results from a mechanistic perspective. Therefore, the main motivation here is not to maximize the fitting between the model results with experimental data, but instead to depict the mechanisms behind the experimental observations in a *Popperian* way, that is, by proposing a possible (though falsifiable) scenario for the observed frequency-specific envelope functional connectivity observed in MEG data (Gamez, 2012). In this simplistic approach, we divided the brain into 90 brain areas; assumed identical 40Hz oscillators with constant amplitude; defined the time-delays as a function of the distance between brain areas; considered a homogeneous propagation speed; and used a simple model of coupled oscillators to simulate the time-delayed phase interactions. In this way, only two parameters may be varied in the model: the global coupling weight and the mean of the delay distribution. Although fine-tuning some model properties – such as the local oscillation frequency or the local transmission speed – may improve the model's performance in estimating real MEG functional connectivity, it is beyond the scope of this work.

In a limited range of model parameters, an optimal fit with experimental data was obtained. In more detail, structured amplitude envelopes of band-pass filtered signals emerged in the system fairly approximating the ones obtained from real MEG data. Namely, the global functional connectivity peaked for envelopes of 10.5–21.5 Hz oscillations; the spatial organization of frequency-specific functional connectivity patterns reproduced significantly the empirical one; and the envelopes fluctuated on a slow time-scale peaking below 0.1 Hz. Taken overall, our results reveal that time-delayed oscillatory interactions, naturally occurring in the brain, may be at the genesis of the structured amplitude envelope fluctuations observed in resting-state MEG data in limited frequency bands.

Making use of the existing literature on coupled oscillators with community structure and/or time-delayed interactions (Niebur et al., 1991; Shanahan, 2010; Wildie and Shanahan, 2012) we have investigated how these slow fluctuations appear in the simulated data. We found that, in the range of parameters where the best agreement with MEG data was found, the system is in a border regime between incoherence and synchrony where metastable partial synchronization occurs. In this regime, a number of "chimera" states – characterized by coexistent synchronized and desynchronized subsystems – are formed. Due to the existence of time delays, synchronized subsystems are more stable at a reduced collective frequency. This collective frequency depends not only on the delays, τ_{np} and the coupling weights C_{np}, but also on the

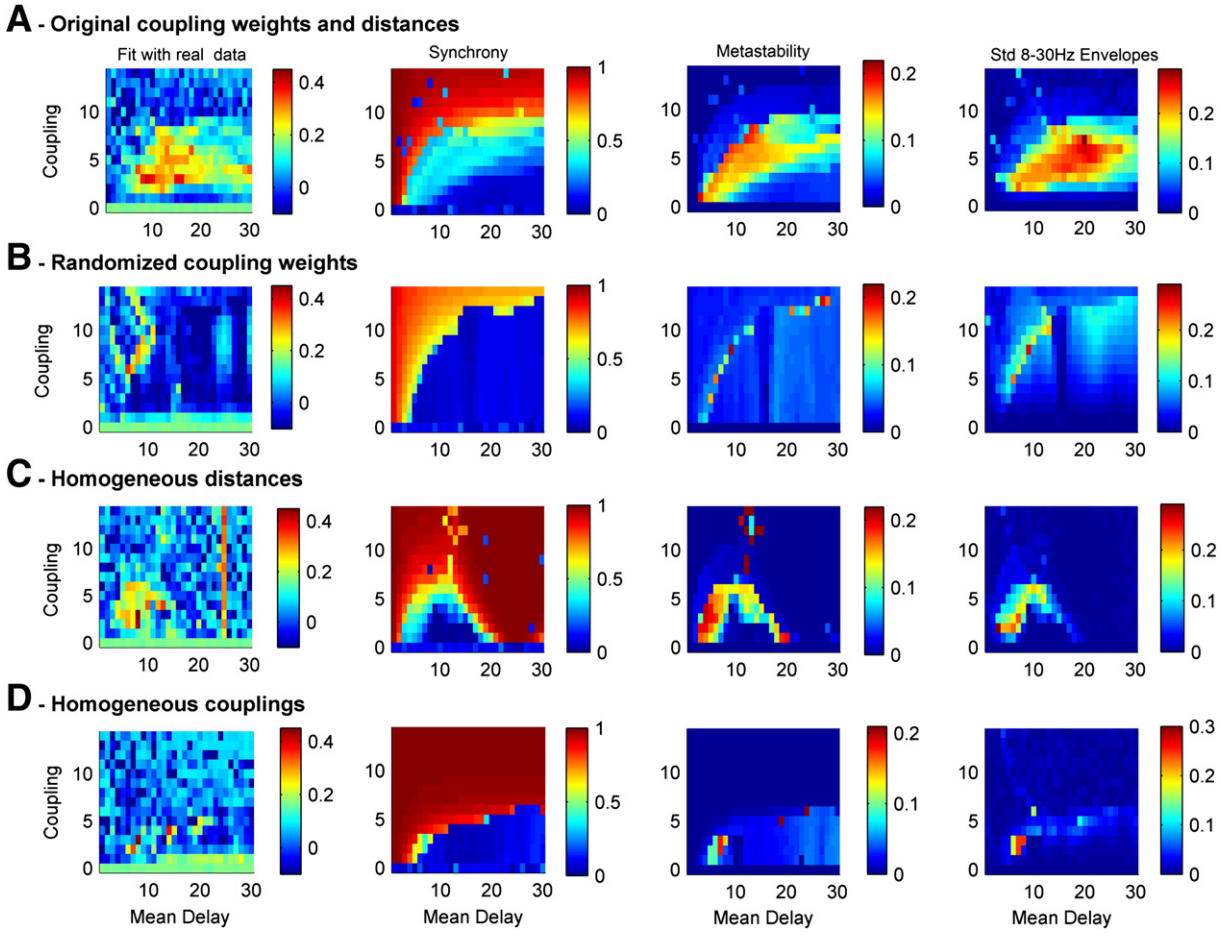

Fig. 6. Role of the brain spatiotemporal network structure on the dynamics. Behavior of the model in the parameter space (same as shown in Fig. 3 A–D) using (A) the original coupling weights derived from DTI and the distances between brain areas, (B) a randomized version of the coupling matrix, (C) the same coupling weights between all connected brain areas and (D) equal distances between all brain areas. Only with the original space-time structure of the brain network, metastable synchronization -and consequently structured envelope fluctuations- occurs for a wide range of model parameters.

natural frequency of the oscillators (ω_n) and the number of nodes in the subsystem. Therefore, multiple, more or less stable, collective frequencies may emerge spontaneously in the system, due to the natural heterogeneity of couplings, delays and natural frequencies in the brain. Due to the characteristics of the model, the frequency modulation is expressed only in the phase of the oscillators while the amplitude is kept constant. The detection of a group of nodes that temporally synchronize together at a given collective frequency can be achieved by band-pass filtering the signals from all nodes around the collective frequency, and identifying the ones that display correlated amplitude fluctuations. Notably, it corresponds to the same method used in experimental studies to estimate spontaneous functional connectivity and detect resting-state functional networks from MEG data. Although the model fairly reproduces the large-scale frequency-specific correlation structure of spontaneous MEG data, it is important to note that the spontaneous oscillatory activity obtained from encephalographic recordings appears to display more than just changes in phase. Incorporating amplitude changes in the local node model may influence the connectivity between phases and affect its dynamical behavior (Daffertshofer and van Wijk, 2011). Therefore, it is important to investigate to what extent the mechanisms proposed herein contribute to the complex dynamics observed in real data using more realistic neural-mass models.

This work proposes a novel generative model for spontaneous brain rhythms, intrinsically shaped by the large-scale space-time structure of the neuroanatomical network. In this scenario, the spontaneous alpha and beta oscillations observed in the brain at rest (the so-called "idle rhythms") would be generated by the temporary large-scale synchronization of certain brain areas at their lowest stable collective frequency (falling in the alpha and beta frequency bands). This is in agreement with the findings from Nikouline et al. (2001), who reported that the synchronization between left and right hemisphere beta-band oscillations was stronger when these oscillations had larger amplitude. However, although MEG has the temporal resolution to capture these frequency-dependent interactions, the detection of in-phase synchronization is largely affected by biases introduced by the source reconstruction approach (such as the one used herein) and additionally confounded with volume conduction effects. Recently, Hillebrand et al. (2012) proposed to use the phase lag index (PLI) to reliably determine MEG functional connectivity from the phase of the reconstructed signals. They found that the brain areas displaying higher PLI in the alpha- and beta-frequency bands also had more power in these frequency bands. To the extent that the PLI may be interpreted as a measure of (phase-lagged) synchronization, these results suggest a close relationship between the degree of synchrony and the power of alpha and beta oscillations in the brain.

Other theoretical models have been proposed for the generation of alpha oscillations. Although the latter could (mechanistically) be generated at the neural population level (Wilson and Cowan, 1972), most scenarios point to the key role of the macroscopic connectivity to generate oscillations in the alpha frequency band (Freyer et al., 2011; Lopes da Silva et al., 1974; Nunez, 2000). In particular, a mechanism for the bi-stable alpha-band activity observed in resting-state cortical recordings (i.e. high power *versus* low power) was proposed using a two-state biophysical model with simplified cortico-thalamic connectivity (Freyer et al., 2011). In the current model, we go further by considering realistic whole-brain brain connectivity (including the cortico-thalamic projections) and show that multiple metastable states may occur, giving rise to spontaneous brain rhythms at different frequencies. The existence of stable reduced collective frequencies shaped by the brain's space-time structure deserves further attention (even beyond spontaneous activity) as it may bring a new light to understand the biophysical mechanisms mediating long-distance functional connectivity in the brain.

In a previous work, and using the same model, we found that resting-state BOLD signal fluctuations were intrinsically related to slow fluctuations in the synchrony degree (Cabral et al., 2011). Here, the analysis was extended to the faster oscillatory dimension revealed by MEG recordings. The new results reinforce the scenario that the brain at rest is operating in a regime of metastable partial synchronization, where the synchrony degree of a given subsystem (or functional network) modulates not only its BOLD signal but also the frequency at which the nodes in the system oscillate. In other words, during periods of lower synchrony, brain areas oscillate in the gamma-band, implying an acceleration of the temporal dynamics which has been shown to cause BOLD signal increases at the local level (Logothetis et al., 2001). During periods of synchronization, the temporal dynamics is slowed down and consequently the BOLD signal is decreased (Kilner et al., 2005; Laufs et al., 2003a). Indeed, the elevated energy requirements of high-frequency neural oscillations represent a mechanistic link between the functional connectivity of brain regions and their respective metabolic demands (Lord et al., 2013; Pfurtscheller et al., 1996). Taken overall, and despite its simplicity, the current model provides a unified picture for the phenomena observed in the spontaneous state at different temporal, spatial and spectral scales.

Acknowledgments

The research reported herein was supported by the ERC Advanced Grant: DYSTRUCTURE (n. 295129), by the FET Flagship Human Brain Project, by the Spanish Research Project SAF2010-16085, by the CONSOLIDER-INGENIO 2010 CSD2007-00012, by the BrainNRG through the James S. McDonnell Foundation, by the FP7-ICT BrainScales, by the RCUK Digital Economy – Centre for Doctoral Training in Healthcare Innovation, by the MINDLab Investment Capital for University Research Fund and by the TrygFonden Charitable Foundation.

Appendix A. Supplementary data

Supplementary data to this article can be found online at http://dx.doi.org/10.1016/j.neuroimage.2013.11.047.

References

Acebron, J.A., Bonilla, L.L., Vicente, C.J.P., Ritort, F., Spigler, R., 2005. The Kuramoto model: a simple paradigm for synchronization phenomena. Rev. Mod. Phys. 77, 137–185.
Baldi, P., Atiya, A.F., 1994. How delays affect neural dynamics and learning. IEEE Trans. Neural Netw. 5, 612–621.
Bartos, M., Vida, I., Jonas, P., 2007. Synaptic mechanisms of synchronized gamma oscillations in inhibitory interneuron networks. Nat. Rev. Neurosci. 8, 45–56.
Behrens, T.E., Woolrich, M.W., Jenkinson, M., Johansen-Berg, H., Nunes, R.G., Clare, S., Matthews, P.M., Brady, J.M., Smith, S.M., 2003. Characterization and propagation of uncertainty in diffusion-weighted MR imaging. Magn. Reson. Med. 50, 1077–1088.
Behrens, T.E., Berg, H.J., Jbabdi, S., Rushworth, M.F., Woolrich, M.W., 2007. Probabilistic diffusion tractography with multiple fibre orientations: what can we gain? Neuroimage 34, 144–155.
Biswal, B., Yetkin, F.Z., Haughton, V.M., Hyde, J.S., 1995. Functional connectivity in the motor cortex of resting human brain using echo-planar MRI. Magn. Reson. Med. 34, 537–541.
Biswal, B.B., Mennes, M., Zuo, X.N., Gohel, S., Kelly, C., Smith, S.M., Beckmann, C.F., Adelstein, J.S., Buckner, R.L., Colcombe, S., Dogonowski, A.M., Ernst, M., Fair, D., Hampson, M., Hoptman, M.J., Hyde, J.S., Kiviniemi, V.J., Kotter, R., Li, S.J., Lin, C.P., Lowe, M.J., Mackay, C., Madden, D.J., Madsen, K.H., Margulies, D.S., Mayberg, H.S., McMahon, K., Monk, C.S., Mostofsky, S.H., Nagel, B.J., Pekar, J.J., Peltier, S.J., Petersen, S.E., Riedl, V., Rombouts, S.A., Rypma, B., Schlaggar, B.L., Schmidt, S., Seidler, R.D., Siegle, G.J., Sorg, C., Teng, G.J., Veijola, J., Villringer, A., Walter, M., Wang, L., Weng, X.C., Whitfield-Gabrieli, S., Williamson, P., Windischberger, C., Zang, Y.F., Zhang, H.Y., Castellanos, F.X., Milham, M.P., 2010. Toward discovery science of human brain function. Proc. Natl. Acad. Sci. U. S. A. 107, 4734–4739.
Borgers, C., Kopell, N., 2003. Synchronization in networks of excitatory and inhibitory neurons with sparse, random connectivity. Neural Comput. 15, 509–538.
Breakspear, M., Heitmann, S., Daffertshofer, A., 2010. Generative models of cortical oscillations: neurobiological implications of the Kuramoto model. Front. Hum. Neurosci. 4.
Brookes, M.J., Hale, J.R., Zumer, J.M., Stevenson, C.M., Francis, S.T., Barnes, G.R., Owen, J.P., Morris, P.G., Nagarajan, S.S., 2011a. Measuring functional connectivity using MEG: methodology and comparison with fcMRI. Neuroimage 56, 1082–1104.
Brookes, M.J., Woolrich, M., Luckhoo, H., Price, D., Hale, J.R., Stephenson, M.C., Barnes, G.R., Smith, S.M., Morris, P.G., 2011b. Investigating the electrophysiological basis of resting state networks using magnetoencephalography. Proc. Natl. Acad. Sci. U. S. A. 108, 16783–16788.

Brookes, M.J., Woolrich, M.W., Barnes, G.R., 2012. Measuring functional connectivity in MEG: a multivariate approach insensitive to linear source leakage. Neuroimage 63, 910–920.

Brunel, N., 2000. Dynamics of sparsely connected networks of excitatory and inhibitory spiking neurons. J. Comput. Neurosci. 8, 183–208.

Brunel, N., Wang, X.J., 2003. What determines the frequency of fast network oscillations with irregular neural discharges? I. Synaptic dynamics and excitation-inhibition balance. J. Neurophysiol. 90, 415–430.

Cabral, J., Hugues, E., Sporns, O., Deco, G., 2011. Role of local network oscillations in resting-state functional connectivity. Neuroimage 57, 130–139.

Collins, D., Neelin, P., Peters, T., Evans, A.C., 1994. Automatic 3D intersubject registration of MR volumetric data in standardized Talairach space. J. Comput. Assist. Tomogr. 18, 192–205.

Daffertshofer, A., van Wijk, B.C., 2011. On the Influence of Amplitude on the Connectivity between Phases. Front. Neuroinformatics 5, 6.

de Munck, J.C., Goncalves, S.I., Huijboom, L., Kuijer, J.P., Pouwels, P.J., Heethaar, R.M., Lopes da Silva, F.H., 2007. The hemodynamic response of the alpha rhythm: an EEG/fMRI study. Neuroimage 35, 1142–1151.

de Pasquale, F., Della Penna, S., Snyder, A.Z., Lewis, C., Mantini, D., Marzetti, L., Belardinelli, P., Ciancetta, L., Pizzella, V., Romani, G.L., Corbetta, M., 2010. Temporal dynamics of spontaneous MEG activity in brain networks. Proc. Natl. Acad. Sci. U. S. A. 107, 6040–6045.

de Pasquale, F., Della Penna, S., Snyder, A.Z., Marzetti, L., Pizzella, V., Romani, G.L., Corbetta, M., 2012. A cortical core for dynamic integration of functional networks in the resting human brain. Neuron 74, 753–764.

Deco, G., Jirsa, V.K., 2012. Ongoing cortical activity at rest: criticality, multistability, and ghost attractors. J. Neurosci. 32, 3366–3375.

Deco, G., Jirsa, V., McIntosh, A.R., Sporns, O., Kotter, R., 2009. Key role of coupling, delay, and noise in resting brain fluctuations. Proc. Natl. Acad. Sci. U. S. A. 106, 10302–10307.

Deco, G., Ponce-Alvarez, A., Mantini, D., Romani, G.L., Hagmann, P., Corbetta, M., 2013. Resting-state functional connectivity emerges from structurally and dynamically shaped slow linear fluctuations. J. Neurosci. 33 (27), 11239–11252. http://dx.doi.org/10.1523/JNEUROSCI.1091-13.2013.

Dhamala, M., Jirsa, V.K., Ding, M., 2004. Enhancement of neural synchrony by time delay. Phys. Rev. Lett. 92, 074104.

Difrancesco, M.W., Holland, S.K., Szaflarski, J.P., 2008. Simultaneous EEG/functional magnetic resonance imaging at 4 Tesla: correlates of brain activity to spontaneous alpha rhythm during relaxation. J. Clin. Neurophysiol. 25, 255–264.

Freyer, F., Roberts, J.A., Becker, R., Robinson, P.A., Ritter, P., Breakspear, M., 2011. Biophysical mechanisms of multistability in resting-state cortical rhythms. J. Neurosci. 31, 6353–6361.

Gamez, D., 2012. From Baconian to Popperian Neuroscience. Neural Syst. Circuits 2, 2.

Ghosh, A., Rho, Y., McIntosh, A.R., Kotter, R., Jirsa, V.K., 2008a. Cortical network dynamics with time delays reveals functional connectivity in the resting brain. Cogn. Neurodyn. 2, 115–120.

Ghosh, A., Rho, Y., McIntosh, A.R., Kotter, R., Jirsa, V.K., 2008b. Noise during rest enables the exploration of the brain's dynamic repertoire. PLoS Comput. Biol. 4, e1000196.

Goldman, R.I., Stern, J.M., Engel Jr., J., Cohen, M.S., 2002. Simultaneous EEG and fMRI of the alpha rhythm. Neuroreport 13, 2487–2492.

Gong, G., Rosa-Neto, P., Carbonell, F., Chen, Z.J., He, Y., Evans, A.C., 2009. Age- and gender-related differences in the cortical anatomical network. J. Neurosci. 29, 15684–15693.

Hagmann, P., Kurant, M., Gigandet, X., Thiran, P., Wedeen, V.J., Meuli, R., Thiran, J.P., 2007. Mapping human whole-brain structural networks with diffusion MRI. PLoS One 2, e597.

Hillebrand, A., Barnes, G.R., Bosboom, J.L., Berendse, H.W., Stam, C.J., 2012. Frequency-dependent functional connectivity within resting-state networks: an atlas-based MEG beamformer solution. Neuroimage 59, 3909–3921.

Hipp, J.F., Hawellek, D.J., Corbetta, M., Siegel, M., Engel, A.K., 2012. Large-scale cortical correlation structure of spontaneous oscillatory activity. Nat. Neurosci. 15, 884–890.

Honey, C.J., Kotter, R., Breakspear, M., Sporns, O., 2007. Network structure of cerebral cortex shapes functional connectivity on multiple time scales. Proc. Natl. Acad. Sci. U. S. A. 104, 10240–10245.

Honey, C.J., Sporns, O., Cammoun, L., Gigandet, X., Thiran, J.P., Meuli, R., Hagmann, P., 2009. Predicting human resting-state functional connectivity from structural connectivity. Proc. Natl. Acad. Sci. U. S. A. 106, 2035–2040.

Huang, M.X., Mosher, J.C., Leahy, R.M., 1999. A sensor-weighted overlapping-sphere head model and exhaustive head model comparison for MEG. Phys. Med. Biol. 44, 423–440.

Jenkinson, M., Bannister, P., Brady, M., Smith, S., 2002. Improved optimization for the robust and accurate linear registration and motion correction of brain images. Neuroimage 17, 825–841.

Jirsa, V.K., 2009. Neural field dynamics with local and global connectivity and time delay. Philos. Transact. A Math. Phys. Eng. Sci. 367, 1131–1143.

Kilner, J.M., Mattout, J., Henson, R., Friston, K.J., 2005. Hemodynamic correlates of EEG: a heuristic. Neuroimage 28, 280–286.

Kitzbichler, M.G., Smith, M.L., Christensen, S.R., Bullmore, E., 2009. Broadband criticality of human brain network synchronization. PLoS Comput. Biol. 5, e1000314.

Knock, S.A., McIntosh, A.R., Sporns, O., Kotter, R., Hagmann, P., Jirsa, V.K., 2009. The effects of physiologically plausible connectivity structure on local and global dynamics in large scale brain models. J. Neurosci. Methods 183, 86–94.

Kuramoto, Y., 1984. Chemical Oscillations, Waves, and Turbulence. Springer-Verlag, Berlin.

Laufs, H., Kleinschmidt, A., Beyerle, A., Eger, E., Salek-Haddadi, A., Preibisch, C., Krakow, K., 2003a. EEG-correlated fMRI of human alpha activity. Neuroimage 19, 1463–1476.

Laufs, H., Krakow, K., Sterzer, P., Eger, E., Beyerle, A., Salek-Haddadi, A., Kleinschmidt, A., 2003b. Electroencephalographic signatures of attentional and cognitive default modes in spontaneous brain activity fluctuations at rest. Proc. Natl. Acad. Sci. U. S. A. 100, 11053–11058.

Liu, Z., Fukunaga, M., de Zwart, J.A., Duyn, J.H., 2010. Large-scale spontaneous fluctuations and correlations in brain electrical activity observed with magnetoencephalography. Neuroimage 51, 102–111.

Logothetis, N.K., Pauls, J., Augath, M., Trinath, T., Oeltermann, A., 2001. Neurophysiological investigation of the basis of the fMRI signal. Nature 412, 150–157.

Lopes da Silva, F.H., Hoeks, A., Smits, H., Zetterberg, L.H., 1974. Model of brain rhythmic activity. The alpha-rhythm of the thalamus. Kybernetik 15, 27–37.

Lord, L.D., Expert, P., Huckins, J.F., Turkheimer, F.E., 2013. Cerebral energy metabolism and the brain's functional network architecture: an integrative review. J. Cereb. Blood Flow Metab. 33, 1347–1354.

Luckhoo, H., Hale, J.R., Stokes, M.G., Nobre, A.C., Morris, P.G., Brookes, M.J., Woolrich, M.W., 2012. Inferring task-related networks using independent component analysis in magnetoencephalography. Neuroimage 62, 530–541.

Mantini, D., Perrucci, M.G., Del Gratta, C., Romani, G.L., Corbetta, M., 2007. Electrophysiological signatures of resting state networks in the human brain. Proc. Natl. Acad. Sci. U. S. A. 104, 13170–13175.

Maslov, S., Sneppen, K., 2002. Specificity and stability in topology of protein networks. Science 296, 910–913.

Niebur, E., Schuster, H.G., Kammen, D.M., 1991. Collective frequencies and metastability in networks of limit-cycle oscillators with time delay. Phys. Rev. Lett. 67, 2753–2756.

Nikouline, V.V., Linkenkaer-Hansen, K., Huttunen, J., Ilmoniemi, R.J., 2001. Interhemispheric phase synchrony and amplitude correlation of spontaneous beta oscillations in human subjects: a magnetoencephalographic study. Neuroreport 12, 2487–2491.

Nir, Y., Mukamel, R., Dinstein, I., Privman, E., Harel, M., Fisch, L., Gelbard-Sagiv, H., Kipervasser, S., Andelman, F., Neufeld, M.Y., Kramer, U., Arieli, A., Fried, I., Malach, R., 2008. Interhemispheric correlations of slow spontaneous neuronal fluctuations revealed in human sensory cortex. Nat. Neurosci. 11, 1100–1108.

Nunez, P.L., 2000. Toward a quantitative description of large-scale neocortical dynamic function and EEG. Behav. Brain Sci. 23, 371–398 (discussion 399–437).

Pfurtscheller, G., Stancak Jr., A., Neuper, C., 1996. Event-related synchronization (ERS) in the alpha band–an electrophysiological correlate of cortical idling: a review. Int. J. Psychophysiol. 24, 39–46.

Pikovsky, A., Rosenblum, M., Kurths, J., 2001. Synchronization: A Universal Concept in Nonlinear Sciences. Cambridge University Press.

Ritter, P., Moosmann, M., Villringer, A., 2009. Rolandic alpha and beta EEG rhythms' strengths are inversely related to fMRI-BOLD signal in primary somatosensory and motor cortex. Hum. Brain Mapp. 30, 1168–1187.

Robinson, S., Vrba, J., 1998. Functional neuroimaging by synthetic aperture magnetometry. Recent Adv. Biomagn. 302–305.

Rubinov, M., Sporns, O., 2010. Complex network measures of brain connectivity: uses and interpretations. Neuroimage 52, 1059–1069.

Shanahan, M., 2010. Metastable chimera states in community-structured oscillator networks. Chaos 20, 013108.

Shmuel, A., Leopold, D.A., 2008. Neuronal correlates of spontaneous fluctuations in fMRI signals in monkey visual cortex: implications for functional connectivity at rest. Hum. Brain Mapp. 29, 751–761.

Strogatz, S., 2003. Sync: The Emerging Science of Spontaneous Order, *Hyperion* (New York).

Taulu, S., Simola, J., Kajola, M., 2005. Applications of the Signal Space Separation Method. IEEE Trans. Sign. Proces. 53, 3359–3372.

Tzourio-Mazoyer, N., Landeau, B., Papathanassiou, D., Crivello, F., Etard, O., Delcroix, N., Mazoyer, B., Joliot, M., 2002. Automated anatomical labeling of activations in SPM using a macroscopic anatomical parcellation of the MNI MRI single-subject brain. Neuroimage 15, 273–289.

Van Veen, B.D., van Drongelen, W., Yuchtman, M., Suzuki, A., 1997. Localization of brain electrical activity via linearly constrained minimum variance spatial filtering. IEEE Trans. Biomed. Eng. 44, 867–880.

Wildie, M., Shanahan, M., 2012. Metastability and chimera states in modular delay and pulse-coupled oscillator networks. Chaos 22, 043131.

Wilson, H.R., Cowan, J.D., 1972. Excitatory and inhibitory interactions in localized populations of model neurons. Biophys. J. 12, 1–24.

Woolrich, M., Hunt, L., Groves, A., Barnes, G., 2011. MEG beamforming using Bayesian PCA for adaptive data covariance matrix regularization. Neuroimage 57, 1466–1479.

Yan, B., Li, P., 2013. The emergence of abnormal hypersynchronization in the anatomical structural network of human brain. Neuroimage 65, 34–51.

Yeung, M.K.S., Strogatz, S.H., 1999. Time delay in the Kuramoto model of coupled oscillators. Phys. Rev. Lett. 82, 648–651.